Quadrupole and magnetic mechanisms of ^{209}Bi spin-lattice relaxation in $Bi_4Ge_3O_{12}$

2002 J. Phys.: Condens. Matter 14 3891

(http://iopscience.iop.org/0953-8984/14/15/304)

INSTITUTE OF PHYSICS PUBLISHING JOURNAL OF PHYSICS: CONDENSED MATTER

J. Phys.: Condens. Matter **14** (2002) 3891–3903 PII: S0953-8984(02)33410-6

Quadrupole and magnetic mechanisms of ^{209}Bi spin–lattice relaxation in $Bi_4Ge_3O_{12}$

A A Gippius[1,4], D F Khozeev[1], E N Morozova[1], V G Orlov[2], M P Shlikov[2] and Yu F Kargin[3]

[1] Moscow State University, 119899, Moscow, Russia
[2] Russian Research Centre Kurchatov Institute, 123182, Moscow, Russia
[3] Institute of General and Inorganic Chemistry, RAS, 117907, Moscow, Russia

E-mail: gippius@mail.ru

Received 5 February 2002
Published 4 April 2002
Online at stacks.iop.org/JPhysCM/14/3891

Abstract

The nuclear spin–lattice relaxation in the $Bi_4Ge_3O_{12}$ single crystal was studied by the ^{209}Bi NQR spin-echo technique. The recovery curves were measured for all ^{209}Bi NQR transitions of nuclear spin $I = 9/2$ in a large temperature range 10–230 K. The experimental relaxation curves were described in terms of the single effective spin–lattice relaxation time T_1^*. The temperature dependence of $1/T_1^*$ was close to a T^n-law with $n = 2.4$–2.7. A theoretical treatment was given for the nuclear spin–lattice relaxation in the multi-level system for the case of a single-axial crystalline electric field. Both quadrupole and magnetic mechanisms of relaxation were taken into account. In separating the quadrupole and magnetic contributions, an idea of Rega (Rega T 1991 *J. Phys.: Condens. Matter* **3** 1871) was used. To extract the temperature dependences of the parameters W_1, W_2 and W_M the fitting procedure for calculated and experimental relaxation times was used. High-accuracy measurements of the recovery curves enable us to conclude that the magnetic mechanism contributes noticeably to the spin–lattice relaxation in $Bi_4Ge_3O_{12}$ at $T \leqslant 50$ K.

1. Introduction

The $Bi_4Ge_3O_{12}$ compound contains neither transition nor rare-earth elements. However, local ordered magnetic fields of about 30 G were revealed in the $Bi_4Ge_3O_{12}$ single crystal by ^{209}Bi NQR experiments [1]. Zero-field splittings showing the typical Zeeman patterns were found earlier in the ^{209}Bi NQR spectra of α-Bi_2O_3 and Bi_3O_4Br (see [2] and references therein). Moreover, spectral patterns of dramatically increased intensity and multiplicity were observed in ^{209}Bi NQR spectra of the $Bi_4Ge_3O_{12}$ single crystal in the presence of a rather weak external dc

[4] Author to whom any correspondence should be addressed.

magnetic field (up to 500 Oe) [1]. The origin of these phenomena is not known yet. Therefore it is of interest to perform ^{209}Bi NQR spin–lattice relaxation experiments on a $Bi_4Ge_3O_{12}$ single crystal to elucidate the nature of the relaxation mechanism (quadrupole or magnetic).

The analysis of spin–lattice relaxation experiments performed by the NQR technique or by the NMR method in the presence of quadrupole effects for nuclei with spins $I \geqslant 5/2$ is complicated because of the multi-exponential nature of the relaxation process in multi-level systems with non-equidistant energy levels [3–9]. In particular, in the case of a single-axial crystalline electric field in $Bi_4Ge_3O_{12}$ there are five doubly degenerate energy levels $|\pm m\rangle$ of ^{209}Bi nuclear spin $I = 9/2$ with transition frequencies between neighbouring levels related as 1:2:3:4 [1]. Therefore the spin–lattice relaxation process in $Bi_4Ge_3O_{12}$ has to be described in terms of four relaxation times T_{1i} $(i = 1, \ldots, 4)$. The quadrupole relaxation times T_{1i} depend on the quantities W_1 and W_2, which are the coefficients in the $\Delta m = \pm 1$ and ± 2 relaxation transition probabilities [10]. The values and temperature dependences of W_1 and W_2 are governed by a specific mechanism of quadrupole relaxation and are *a priori* unknown.

Further problems arise when the magnetic mechanism competes with the quadrupole one in the spin–lattice relaxation process [11–13]. A third unknown quantity W_M, which is a coefficient in the $\Delta m = \pm 1$ magnetic relaxation transition probability [3], also affects the relaxation times T_{1i} in this case.

To avoid the difficulties of a full-scale treatment of the relaxation process in the multi-level systems, an elegant method for separating the magnetic and quadrupole rates by analysing the recovery plots at $t \to 0$ was proposed by Rega [11]. However, the procedure proposed in [11] seems to be oversimplified. In this paper we use the idea of Rega [11] and present a complete experimental and theoretical treatment of the relaxation mechanisms in $Bi_4Ge_3O_{12}$.

2. Experimental procedure

The $Bi_4Ge_3O_{12}$ single crystals were grown in air from a stoichiometric melt. The pulling process was performed by the Czochralski method using a platinum crucible 90 mm in diameter and 200 mm in height for charging. The starting charge for growth was prepared by solid-state synthesis from extra-pure bismuth oxide and germanium oxide, both alpha allotropes. The solid-state chemical reactions were conducted in platinum crucibles in three stages: pre-sintering of the starting mixture at 790 °C for 70 h followed by synthesis at 850 and 950 °C for a total of 100 h. The weight of the starting load was 4–5 kg. Crystallographic [001]- or [111]-oriented seed crystals were used. The pulling rate was 1–3 mm h^{-1} and the crystal rotation rate was 10–30 rpm. Colourless, transparent crystal boules 40 mm in diameter and 200 mm in length were grown. For NQR relaxation experiments a sample with size $4 \times 4 \times 10$ mm was used. The longest side of the crystal coincided with the axis of the radio-frequency coil.

NQR experiments were performed using a home-built coherent pulsed spectrometer equipped with a closed-cycle cryogenic refrigerator, JANIS CCS-550, with the operation temperature range 9–300 K. The ^{209}Bi NQR spectra were measured using a frequency step point-by-point spin-echo technique. To avoid echo distortions from the free induction decay (FID) and ringing, a simple two-phase cycling sequence was used. The spin–lattice relaxation rate was measured using the saturation–recovery method at frequencies of different quadrupole transitions of ^{209}Bi nuclear spins. The saturation pulse train consists of 100 pulses of 4 μs with a pulse delay of 30 μs.

Recovery curves were measured for all ^{209}Bi transitions. As an example, recovery curves for the 1/2–3/2 transition at different temperatures are shown in figure 1. The time delay t between the saturation pulse train and the spin-echo sequence covers more than six decades. At temperatures below 150 K the initial saturation is perfect. All recovery curves are successfully

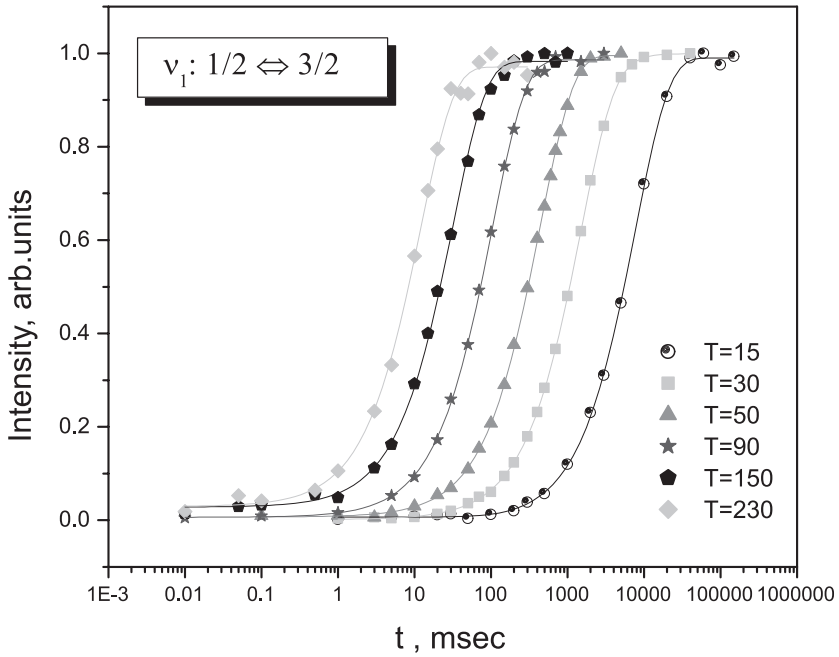

Figure 1. Recovery curves of ^{209}Bi in $Bi_4Ge_3O_{12}$ at different temperatures for the 1/2–3/2 transition. Solid curves show the best fits to the formula (18) (see the text).

fitted by a one-exponential function with characteristic time T_1^*. The extracted effective relaxation rates $R_{1i}^* = 1/T_{1i}^*$ for all ^{209}Bi transitions as functions of temperature are presented in figure 2. The temperature dependences of $1/T_{1i}^*$ are close to a T^n-law with $n = 2.4$–2.7.

3. Theoretical treatment of the nuclear spin–lattice relaxation process for the single-axial crystalline electric field and the spin $I = 9/2$

The Bi atoms occupy the c-type sites located on the threefold rotation axes in the eulitine-type structure of the $Bi_4Ge_3O_{12}$ crystal with electric field gradient (EFG) asymmetry parameter $\eta = 0$. The frequencies of the transitions between the five doubly degenerate energy levels $|\pm m\rangle (m = 1/2, \ldots, 9/2)$ of the spin $I = 9/2$ are multiples of the frequency ν_Q:

$$\nu_Q = 3eQq_{zz}/[2I(2I-1)]h, \tag{1}$$

where eQ is the nuclear quadrupole moment, q_{zz} is the maximum component of the EFG tensor. Since in $Bi_4Ge_3O_{12}$ the local magnetic fields are rather weak [1], their influence on the eigenfunctions of the nuclear spins can be ignored. The theoretical study of the relaxation process is based on the master equation [10]:

$$\frac{dN_i}{dt} = \sum_j (W_{ij}N_j - W_{ji}N_i), \tag{2}$$

where N_i is the population of the ith level, W_{ij} is the probability of transition from the jth to the ith level, the sum over j is taken for all allowed transitions ($\Delta m = \pm 1$ and ± 2) between the levels. The probabilities for these transitions were calculated using the formulae [5]

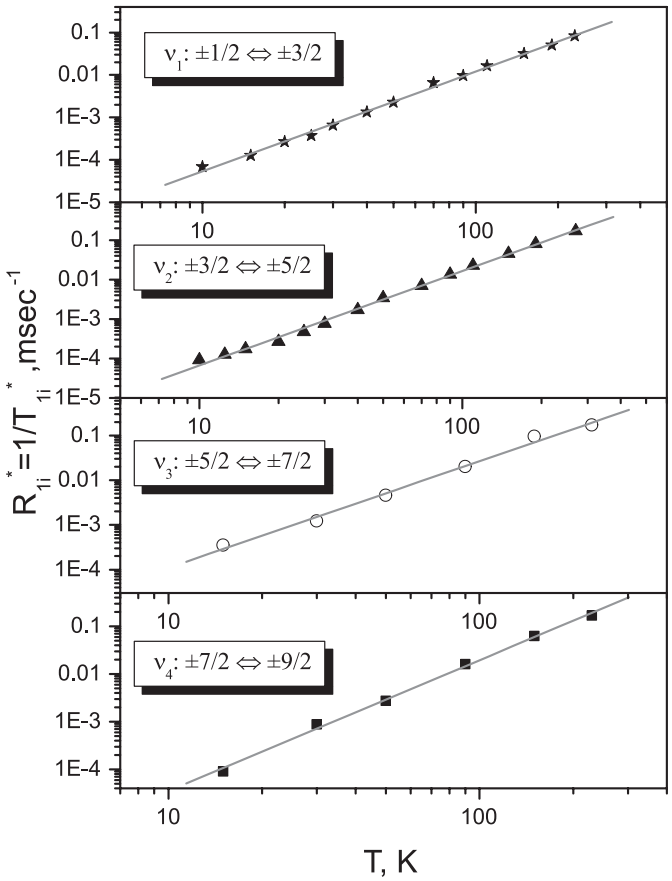

Figure 2. Relaxation rates $R^*_{1i} = 1/T^*_{1i}$ for the quadrupole transitions as functions of temperature. Solid lines show the power law $R_1 = T^n$ with $n = 2.4, 2.4, 2.4, 2.7$ for the $\nu_1, \ldots, \nu_4$ transitions, respectively.

$$W_{m\pm1,m} = \frac{(2m \pm 1)^2 (I \mp m)(I \pm m + 1)}{2I^2(2I-1)^2} W_1, \tag{3}$$

$$W_{m\pm2,m} = \frac{(I \mp m)(I \mp m - 1)(I \pm m + 1)(I \pm m + 2)}{2I^2(2I-1)^2} W_2, \tag{4}$$

where W_1 and W_2 are unknown quantities. The temperature dependences of W_1 and W_2 are determined by comparison of the calculated and experimental relaxation rates.

The transition probabilities for the $\Delta m = \pm 1$ magnetic relaxation processes were defined in [3]:

$$W^M_{m\pm1,m} = W_M (I \mp m)(I \pm m + 1). \tag{5}$$

The temperature dependence of W_M can also be determined by comparison of the calculated and experimental relaxation rates. One should take into account that the transition probabilities from upper levels to lower ones differ from the probabilities for corresponding backward transitions by the factor $\exp(\zeta\Delta) \approx 1 + \zeta\Delta$ (where $\Delta = h\nu_Q/kT \ll 1$, $\zeta = 1, 2, \ldots, 5, 7$).

The differences of the level populations are defined as follows:

$$\begin{aligned} n_{\pm1} &= N_{\pm1/2} - N_{\pm3/2}; & n_{\pm2} &= N_{\pm3/2} - N_{\pm5/2}; \\ n_{\pm3} &= N_{\pm5/2} - N_{\pm7/2}; & n_{\pm4} &= N_{\pm7/2} - N_{\pm9/2}; \\ n_{+i} &= n_{-i}; & N_{+i} &= N_{-i}. \end{aligned} \tag{6}$$

Subtracting the corresponding pairs of equations (2), one can write the resulting rate equations in the following form (see in [5] an example of a similar procedure for the spin 5/2):

$$\dot{n}_1 + (8 + 71\gamma + 8\sqrt{6}\beta)n_1 + 2\tilde{p}_1 n_1 - (14 - 7\gamma + 2\sqrt{21}\beta)n_2 - 14\gamma n_3 = n_0(-20 + 43\gamma + 4(2\sqrt{6} - \sqrt{21})\beta); \tag{7}$$

$$\dot{n}_2 - 4(1 + \gamma + \sqrt{6}\beta)n_1 - \tilde{p}_1 n_1 + (28 + 35\gamma + 4\sqrt{21}\beta)n_2 - 8(3 - \gamma + \beta)n_3 - 6\gamma n_4 = 2n_0(-10 + 33\gamma + 2(2\sqrt{21} - 6 - \sqrt{6})\beta); \tag{8}$$

$$\dot{n}_3 - 21\gamma n_1 - (14 + 7\gamma + 2\sqrt{21}\beta)n_2 + 4(12 + 5\gamma + 4\beta)n_3 - 6(4 - \gamma + \beta)n_4 = n_0(20 + 49\gamma + 4(6 - \sqrt{21})\beta); \tag{9}$$

$$\dot{n}_4 - 14\gamma n_2 - 8(3 + \gamma + \beta)n_3 + 6(8 + \gamma + 2\beta)n_4 = 4n_0(30 - 7\gamma + 6\beta). \tag{10}$$

In equations (7)–(10) $\dot{n}_i = \mathrm{d}n_i/\mathrm{d}\tau$ $(i = 1, \ldots, 4)$, $\tau = tW_1/108$, $\gamma = W_2/W_1$, $\beta = 54W_M/W_1$, $n_0 = \Delta N/5$; $\tilde{p}_1 = 108p_1/W_1$, N is the total number of nuclei. When writing (7) and (8), it was assumed that H_{rf} saturates the transition between the $|\pm1/2\rangle$ and $|\pm3/2\rangle$ levels. Since the resonance radio-frequency field $\boldsymbol{H}_{rf} \parallel \boldsymbol{x}$ (x is the axis of the RF coil), the probability p_1 of a transition between $|\pm1/2\rangle$ and $|\pm3/2\rangle$ levels is proportional to the square of the matrix element $|\langle\pm3/2|H_{rfx}I_x|\pm1/2\rangle|^2 = 6H_{rfx}^2$. In the case of saturation of the 3/2–5/2 transition, the terms $-\tilde{p}_2 n_2, 2\tilde{p}_2 n_2, -\tilde{p}_2 n_2$ should appear in equations (7)–(9) instead of $\tilde{p}_1 n_1$. Similar modifications can be made for the 5/2–7/2 and 7/2–9/2 transitions in (7)–(10).

Equations (7)–(10) enable one to study numerically the relaxation process for the nuclear spin $I = 9/2$ in the case of single-axial electric field. In particular, it is possible to extract the initial values n_{i0}, assuming that the influence of H_{rf} leads to the steady-state picture. By setting $\dot{n}_i = 0$ in (7)–(10), we obtain a system of linear non-uniform algebraic equations for n_{i0}. For the case of pure quadrupole relaxation ($\beta = 0$) it is possible to find an analytical solution of this system, suggesting that the probabilities of transitions caused by H_{rf} are much larger than those of the relaxation transitions:

$$\begin{aligned} n_{10} &= 0; & n_{20} &= \frac{n_0(192 + 832\gamma + 592\gamma^2 + 63\gamma^3)}{96 + 344\gamma + 218\gamma^2 + 21\gamma^3}; \\ n_{30} &= \frac{n_0(288 + 1032\gamma + 570\gamma^2 + 42\gamma^3)}{96 + 344\gamma + 218\gamma^2 + 21\gamma^3}; & n_{40} &= \frac{n_0(384 + 1376\gamma + 872\gamma^2 + 105\gamma^3)}{96 + 344\gamma + 218\gamma^2 + 21\gamma^3}. \end{aligned} \tag{11}$$

When both γ and β are non-zero, n_{i0} can be found by a standard numerical procedure.

The solutions of the uniform system of linear differential equations can be expressed in a simple form: $n_i = a_i \mathrm{e}^{-\lambda\tau}$ $(i = 1, \ldots, 4)$. Substituting these solutions into (7)–(10) with zero right-hand parts and the terms with $\tilde{p}_1$, it is possible to get a system of linear uniform algebraic equations for the coefficients a_i. The characteristic equation of this system enables one to find the relaxation rates $\lambda_i = T_{1i}^{-1}$ $(i = 1, \ldots, 4)$ as functions of γ and β:

$$\begin{vmatrix} 8 + 71\gamma + 8\sqrt{6}\beta - \lambda & -14 + 7\gamma - 2\sqrt{21}\beta & -14\gamma & 0 \\ -4(1 + \gamma + \sqrt{6}\beta) & 28 + 35\gamma + 4\sqrt{21}\beta - \lambda & -8(3 - \gamma + \beta) & -6\gamma \\ -21\gamma & -14 - 7\gamma - 2\sqrt{21}\beta & 4(12 + 5\gamma + 4\beta) - \lambda & -6(4 - \gamma + \beta) \\ 0 & -14\gamma & -8(3 + \gamma + \beta) & 6(8 + \gamma + 2\beta) - \lambda \end{vmatrix} = 0. \tag{12}$$

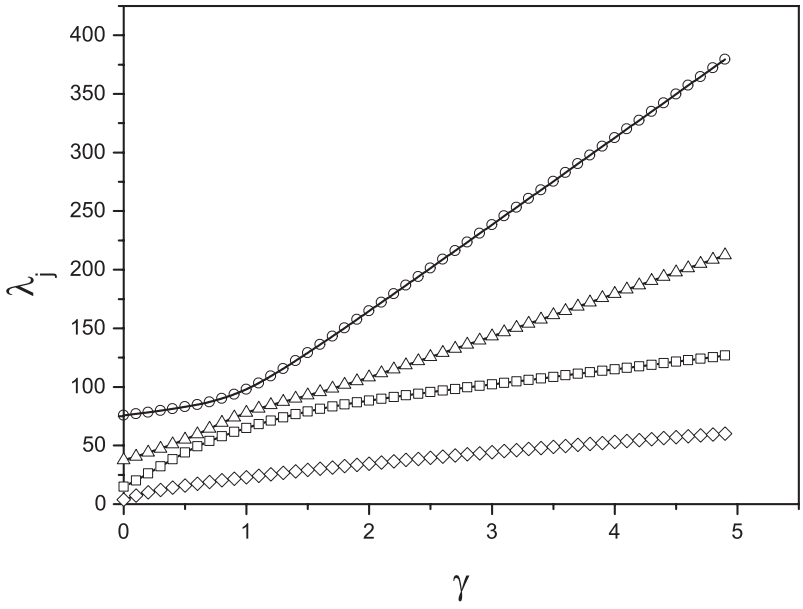

Figure 3. Relaxation rates λ_j for $j = 1$ (◇), $j = 2$ (□), $j = 3$ (△), $j = 4$ (○) as functions of γ for $\beta = 0$. Solid curves are a guide for the eye.

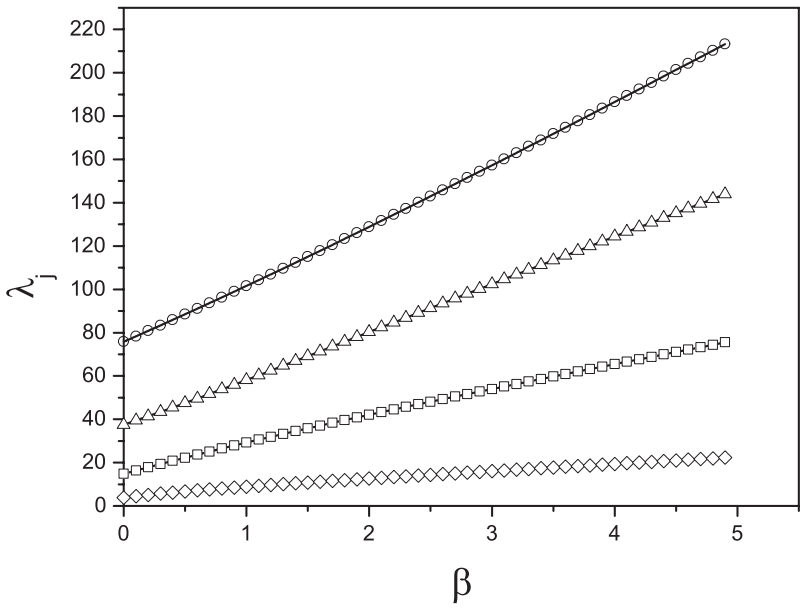

Figure 4. Relaxation rates $\lambda_j (j = 1 \ldots 4)$ as functions of β for $\gamma = 0$. The symbol notation is the same as in figure 3. Solid curves are a guide for the eye.

This equation can be solved numerically. Figures 3 and 4 show the specific solutions $\lambda_j = \lambda_j(\gamma)$ at $\beta = 0$ and $\lambda_j = \lambda_j(\beta)$ at $\gamma = 0$, respectively. As follows from figures 3 and 4, the relaxation rates λ_j are fast-growing non-intersecting functions of γ and β. When both γ and β are non-zero, the character of the functional dependence of λ_j is preserved.

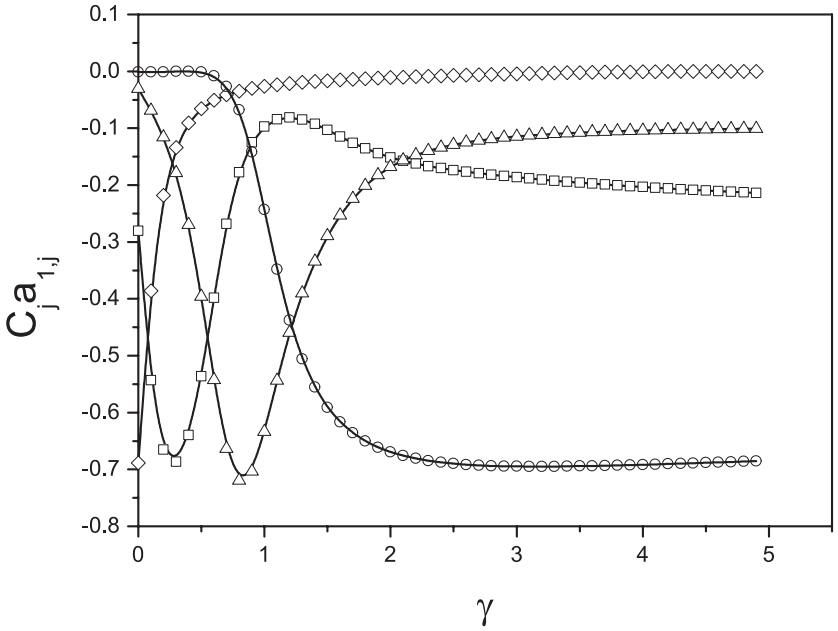

Figure 5. Pre-exponential factors $c_j a_{1j}$ (13) as functions of γ for $\beta = 0$. The symbol notation is the same as in figure 3. Solid curves are a guide for the eye.

The solution of the non-uniform system (7)–(10), which describes the relaxation process for $\tau > 0$ and for H_{rf} switched off ($\tilde{p}_1 = 0$), can be written in the following form:

$$\frac{n_i}{n_0} = \alpha_i + \sum_{j=1}^{4} c_j a_{ij} \mathrm{e}^{-\lambda_j \tau}, \qquad i = 1, \ldots, 4. \tag{13}$$

Here $\alpha_1 = 1, \ldots, \alpha_4 = 4$, $\lambda_j (j = 1, \ldots, 4)$ are solutions of equation (12), a_{ij} are normalized eigenfunctions corresponding to eigenvalues λ_j, the coefficients c_j are determined using the initial conditions for n_i:

$$\frac{n_{i0}}{n_0} = \alpha_i + \sum_{j=1}^{4} c_j a_{ij}, \tag{14}$$

The pre-exponential factors $c_j a_{ij}$ in (13) are functions of the parameters γ and β, as well as the relaxation rates λ_j. As an example, figures 5 and 6 show the dependences of $c_j a_{1j}$ on γ at $\beta = 0$ and 3, respectively. It is worth noting a peculiarity of the relaxation process: while the values of λ_j determine the timescale of the relaxation, the pre-exponential factors $c_j a_{ij}$ are responsible for the form of the relaxation curve. To show this, we rearranged formula (13), taking it into account that $n_{i0} = 0$ when the ith transition is saturated (see for example (11)). Then from (14),

$$\alpha_i = -\sum_{j=1}^{4} c_j a_{ij}. \tag{15}$$

Substituting α_i from (15) into (13), we obtain

$$\frac{n_i}{n_0} = -\sum_{j=1}^{4} c_j a_{ij} (1 - \mathrm{e}^{-\lambda_j \tau}). \tag{16}$$

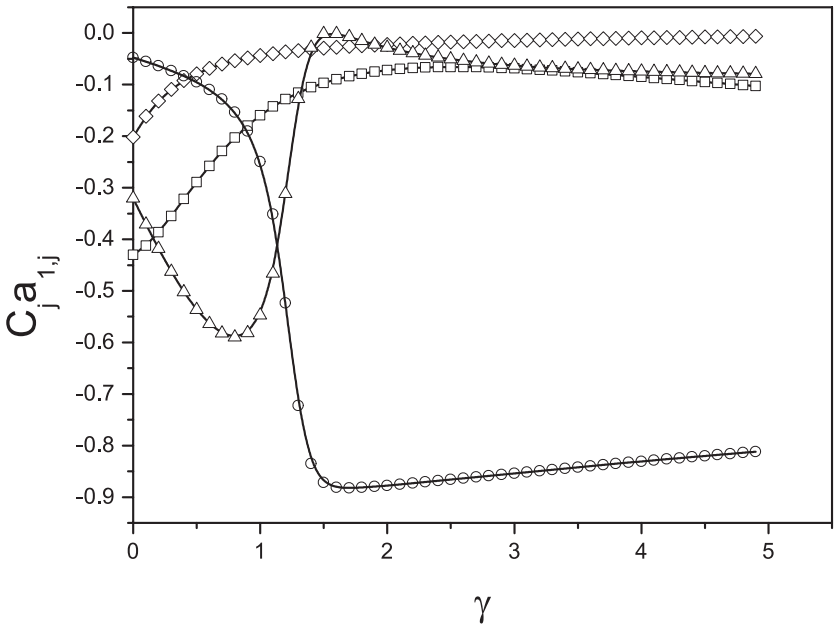

Figure 6. Pre-exponential factors $c_j a_{1j}$ (13) as functions of γ for $\beta = 3$. The symbol notation is the same as in figure 3. Solid curves are a guide for the eye.

The ratio n_i/n_0 (16) consists of four partial contributions:

$$-c_j a_{ij}(1 - \mathrm{e}^{-\lambda_j \tau}). \tag{17}$$

The time evolutions of (17) for $i = 1$, $\beta = 0$ and $\gamma = 1$ are shown in figure 7. From figures 3, 5 and 7 it is clear that the values of the contributions depend mainly on the factors $c_j a_{ij}$. Moreover, when there is no significant difference between the values of the relaxation rates λ_j, the resulting relaxation curve is rather smooth. Therefore the analysis of experimental recovery curves may be ambiguous. To avoid this difficulty, we used the idea of Rega [11] to consider the relaxation process in an early stage.

The experimental recovery curves for all of the ^{209}Bi NQR transitions in the $Bi_4Ge_3O_{12}$ were approximated by the following expression:

$$Y_i = Y_{0i} + A_i(1 - \mathrm{e}^{-t/T_{1i}^*}), \tag{18}$$

where $i = 1, \ldots, 4$ correspond to transitions 1/2–3/2, ..., 7/2–9/2, respectively. The values of T_{1i}^* for a number of temperatures in the range 10–300 K are presented in table 1. The effective experimental relaxation rate for each transition, $R_{1i}^* = 1/T_{1i}^*$, is defined by

$$\left(\frac{\mathrm{d}}{\mathrm{d}t}\frac{Y_i - Y_{0i}}{A_i}\right)_{t=0} = \frac{1}{T_{1i}^*}. \tag{19}$$

An effective calculated relaxation time $T_1^{(i)}$ for the ith transition is defined by the derivative of (13) or (16):

$$\left(\frac{\mathrm{d}}{\mathrm{d}t}\frac{n_i}{\alpha_i n_0}\right)_{t=0} = -\frac{W_1}{\alpha_i \times 108}\sum_{j=1}^{4} a_{ij}c_j\lambda_j \equiv \frac{1}{T_1^{(i)}}, \tag{20}$$

The factor α_i appears in the denominator of formula (20) due to the normalization of the calculated relaxation curve to unity at $t \to \infty$ for each transition. A program for numerical calculations of $T_1^{(i)}$ as a function of the three parameters W_1, γ and β was developed.

Table 1. . Effective experimental (T_{1i}^*) and calculated ($T_1^{(i)}$) relaxation times ($i = 1, \ldots, 4$) for all NQR transitions at different temperatures. The errors for T_{1i}^* include both the fitting and instrumental errors.

	T_1 (ms)	$T = 10$ K	$T = 15$ K	$T = 30$ K	$T = 40$ K	$T = 50$ K	$T = 70$ K	$T = 90$ K	$T = 150$ K	$T = 230$ K
1/2–3/2	T_{11}^*	14 700 ± 400	7850 ± 150	1530 ± 15	760 ± 10	440 ± 5	154 ± 4	104 ± 3	32 ± 1	12.0 ± 0.7
	$T_1^{(1)}$	13 900	6690	1540	751	420	154	104	32.3	12.6
3/2–5/2	T_{12}^*	10 900 ± 500	5800 ± 150	1300 ± 25	580 ± 30	295 ± 20	142 ± 3	74 ± 2	22.0 ± 0.5	12.0 ± 0.7
	$T_1^{(2)}$	12 710	5950	1230	599	320	132	73	19.3	8.8
5/2–7/2	T_{13}^*	17 300 ± 1200	2900 ± 170	830 ± 30	495 ± 20	220 ± 15	88 ± 5	50 ± 2	10.6 ± 0.4	5.9 ± 0.3
	$T_1^{(3)}$	12 230	5030	940	509	260	104	53	13.3	6.3
7/2–9/2	T_{14}^*	12 800 ± 1900	11 000 ± 900	1140 ± 50	600 ± 15	365 ± 30	134 ± 7	61 ± 13	16 ± 1	6.0 ± 0.8
	$T_1^{(4)}$	14 710	6100	1090	589	300	124	59	14.4	7.1

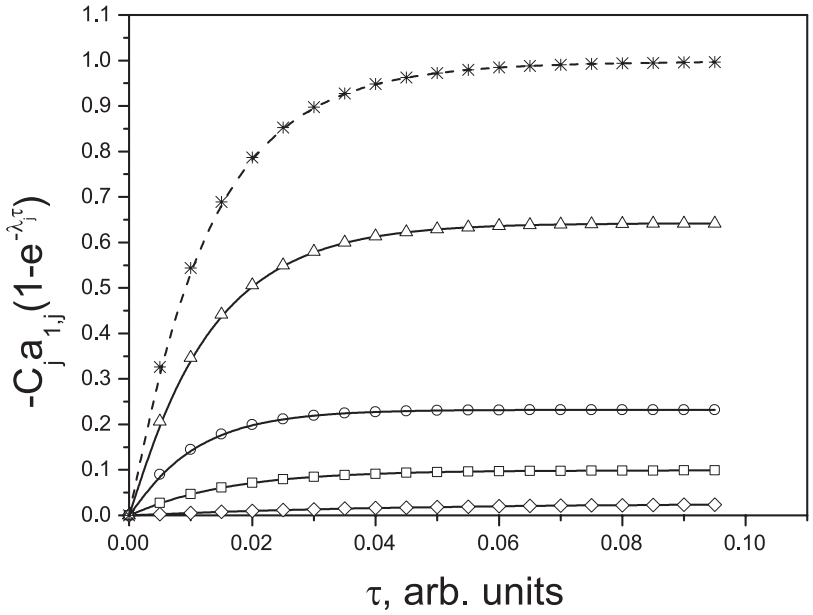

Figure 7. Evolution in time of the partial contributions (17) to the relaxation curve for the first NQR transition 1/2–3/2 calculated with $\beta = 0$ and $\gamma = 1$. The symbol notation is the same as in figure 3. The sum of the partial contributions (16) is denoted by $*$. Solid curves are a guide for the eye.

The procedure of fitting the effective relaxation times T_{1i}^{*} and $T_1^{(i)}$ was carried out numerically to define the temperature dependence of the parameters W_1, W_2 and W_M. As a criterion for the fitting procedure, the minimum of the following expression was used:

$$S = \sum_{i=1}^{4} \frac{(T_{1i}^{*} - T_1^{(i)})^2}{T_{1i}^{*}}. \tag{21}$$

The values of $T_1^{(i)}$ corresponding to the best fit are presented in the table 1. The temperature dependences of the parameters W_1, W_2 and W_M are shown in figure 8.

4. Results and discussion

As follows from table 1, at $T \geqslant 30$ K the calculated values of $T_1^{(i)}$ correctly reproduce the experimentally observed sequence of effective relaxation times for all transitions examined, $T_{11}^{*} > T_{12}^{*} > T_{13}^{*} < T_{14}^{*}$. It must be noted that the number of fitting parameters (W_1, W_2, W_M) was less than the number of independent experiments. Both of these facts can be regarded as evidence of the reliability of the procedure, described by the formulae (18)–(21). The fitting procedure (21) enabled us to extract the parameters W_1, W_2 and W_M at each temperature (see figure 8).

The effective calculated relaxation rates $1/T_1^{(i)}$ (20) clarify the meaning of the effective experimental relaxation rates R_{1i}^{*} for the multi-level system as the weighted sum of the 'true' relaxation rates λ_j.

At low temperatures ($T \leqslant 15$ K), when the effective relaxation times T_{1i}^{*} increase sharply, the character of the relaxation process also changes. For example, at 15 K the largest value among the T_{1i}^{*} is T_{14}^{*} (see table 1), while at 10 K T_{13}^{*} attained the maximum value, which does

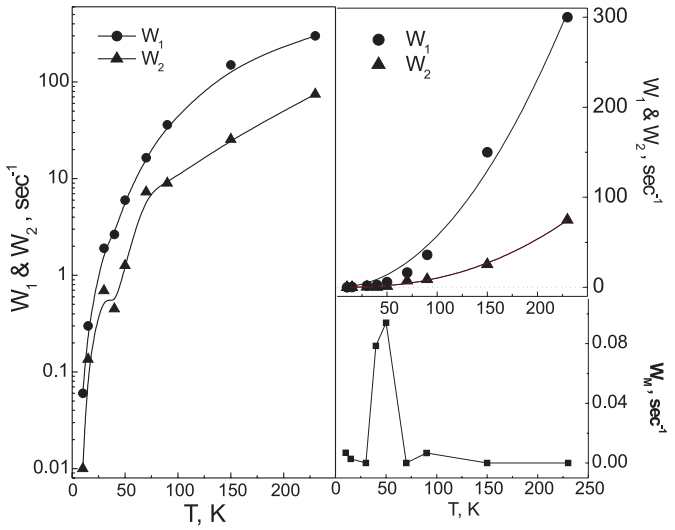

Figure 8. The temperature dependences of the parameters W_1, W_2 on a logarithmic y-scale (left panel) and a linear y-scale (right panel, top) and the parameter W_M (right panel, bottom). Solid curves show the best fits to the power law $W(T) \sim T^n$ with $n = 2.0(1)$ for W_1 and $n = 2.4(1)$ for W_2. In the $W_M(T)$ plot the solid curve is a guide for the eye.

not agree with the above-mentioned relation of relaxation times observed at $T \geqslant 30$ K. As a consequence, the fitting procedure for S (21) at 15 and 10 K gives $T_1^{(i)}$-values which differ markedly from the experimentally observed T_{1i}^* (see table 1). The origin of this behaviour at $T \leqslant 15$ K is not clear yet.

The problem of separation of quadrupole and magnetic contributions in spin–lattice recovery laws was discussed [11, 12] in the context of the magnetic properties of high-T_c superconductors and related compounds. A detailed treatment of this problem was given by Brinkmann and co-workers [13] for the case of a quadrupole-perturbed Zeeman Hamiltonian in the presence of mixed magnetic and quadrupole fluctuations, which is contrary to our case. The authors conclude that it is not possible to separate magnetic and quadrupole contributions to the relaxation rate if the experimental error is above 10%. The 'dominant' contribution (quadrupole or magnetic) determines the relaxation process; therefore the time evolution of the multi-level system to the equilibrium state can be described in terms of a single time constant, T_1^{eff}.

In our case we took advantage of the high symmetry of Bi sites in the $Bi_4Ge_3O_{12}$ crystal lattice and the weakness of the local magnetic fields found in this compound [1]. This enabled us to use the formulae (3)–(5) for calculations of transition probabilities. In table 1 the resulting errors for the effective relaxation times T_{1i}^* are presented—which include both the accuracy of the experimental data fitting by the formula (18) and an instrumental error. As follows from table 1, these errors were predominantly at the level of 5% or less. High experimental accuracy made it possible for us to estimate the typical acceptable range of variance of the parameters W_1, W_2 and W_M at the level of 20–25% of their values determined on the basis of our fitting procedure (21).

As follows from figure 8, the parameters W_1 and W_2 grow rapidly—close to the parabolic law—which is similar to the temperature behaviour of the experimental effective relaxation rates R_{1i}^* (see figure 2). The proportionality $W_1 \sim 1/T_1^{(i)}$ follows from the definition (20). It must be noted that throughout the temperature range studied, 10–230 K, the values of the W_2-

parameter were noticeably smaller than those of W_1. So the magnitude of the ratio $\gamma = W_2/W_1$ never exceeded 0.5. In some previous works, γ was taken equal to 1 (see, for example [11,12]).

The bottom right panel in figure 8 shows the temperature dependence of W_M. On the basis of the results obtained, we can conclude that at $T \geqslant 70$ K the spin–lattice relaxation in $Bi_4Ge_3O_{12}$ is governed mainly by the quadrupolar mechanism. At 50, 40, 15 and 10 K the contribution of the magnetic mechanism is quite noticeable. According to (5), the probabilities of transitions governed by the magnetic mechanism attain rather large values and the parameter β in the rate equations (7)–(10) is defined as $54W_M/W_1$. At low temperatures, when W_1 is not large (figure 8), even small values of W_M contribute significantly to the relaxation. However, in the temperature range $T \geqslant 70$ K, where W_1 and W_2 increase by more than two orders of magnitude as compared with those at 10 K, the parameter β plays a minor role in the rate equations. It is worth noting that in La_2CuO_4, in which there is the antiferromagnetically ordered subsystem of Cu spins at $T < T_N \sim 300$ K, the magnetic relaxation process becomes dominant in the temperature range ($T < 50$ K) [12] where the magnetic mechanism contributes noticeably to the relaxation process in $Bi_4Ge_3O_{12}$.

For the quadrupolar mechanism of relaxation caused by acoustic phonons, the following temperature dependence of the relaxation rate should be observed [10]: $1/T_1 \sim T^2$ at $T \geqslant \theta_D$ and $1/T_1 \sim T^7$ at $T < 0.02\theta_D$, where θ_D is the Debye temperature. For $Bi_4Ge_3O_{12}$, $\theta_D = 236$ K [14], so we were not able to find a sharp drop of the relaxation rate at $T < 0.02\theta_D$ because the lowest temperature of the experiment was 10 K. The measured effective relaxation rates $1/T_{1i}^*$ obeyed the power law T^n with $n = 2.4$ for the first three quadrupole transitions and, for the upper (7/2–9/2) transition, n was equal to 2.7 over the temperature range studied, 10–230 K (see figure 2). The deviation of n from 2 in the observed power law could be attributed to the optic phonon contribution to the quadrupolar mechanism of relaxation for the temperature range $T \sim \theta_D$ in which these vibrational modes are populated (for $Bi_4Ge_3O_{12}$ the frequencies of the lowest registered Raman- and IR-active optic modes are equal to 92 and 63 cm^{-1} [15], respectively). The reason for the universality of the power law T^n for the effective relaxation rates in the large temperature interval 10–230 K is not known yet. It is notable that for La_2CuO_4 at $T > 70$ K, the relaxation rate is also proportional to T^2 [12] even though $\theta_D \sim 400$ K for this compound.

The existence of paramagnetic centres, presumably holes in the unfilled p-electron shell of oxygen ions, was proposed as the origin of the observed magnetoelectric effect in the α-Bi_2O_3 single crystal. This effect is linear with respect to external magnetic field [16,17]. The holes possess a magnetic moment due to spin and orbital magnetic moments. It is quite possible that a similar intrinsic system of paramagnetic centres exists in $Bi_4Ge_3O_{12}$. Tunnelling of holes between several equilibrium positions accompanied by changes of their magnetic state can be regarded as the cause of the local magnetic field fluctuations in $Bi_4Ge_3O_{12}$ at low temperatures. This leads to a noticeable contribution of the magnetic mechanism to the nuclear spin–lattice relaxation, which is observed in our experiment. Unfortunately, the origin of the sharp peak in the temperature dependence of W_M is not clear yet.

5. Conclusions

It was demonstrated that for the case of a single-axial crystalline electric field and a weak local magnetic field realized in $Bi_4Ge_3O_{12}$ it is possible to separate the contributions of quadrupolar and magnetic mechanisms to the relaxation. The experimental recovery curves for the relaxation in a multi-level system were successfully described in terms of a single effective relaxation rate $1/T_1^*$, which is the weighted sum of the 'true' relaxation rates. The temperature dependence of $1/T_1^*$ was described by a T^n-law with $n = 2.4$–2.7 over a large temperature

range 10–230 K. The spin–lattice relaxation in $Bi_4Ge_3O_{12}$ at $T > 70$ K is governed mainly by the quadrupolar mechanism, while at low temperatures the contribution of the magnetic mechanism is noticeable.

Acknowledgments

The authors are grateful to Dr E A Kravchenko for useful discussion. AAG is grateful to INTAS project 99-0155 for partial support.

References

[1] Kravchenko E A, Kargin Yu F, Orlov V G, Okuda T and Yamada K 2001 *J. Magn. Magn. Mater.* **224** 249
[2] Kravchenko E A and Orlov V G 1994 *Z. Naturf.* a **49** 418
[3] Andrew E R and Tunstall D P 1961 *Proc. Phys. Soc.* **78** 1
[4] Tewari D P and Verma G S 1963 *Phys. Rev.* **129** 1975
[5] Daniel A C and Moulton W G 1964 *J. Chem. Phys.* **41** 1833
[6] Narath A 1967 *Phys. Rev.* **162** 320
[7] MacLaughlin D E, Williamson J D and Butterworth J 1971 *Phys. Rev.* B **4** 60
[8] Gordon M I and Hoch M J R 1978 *J. Phys. C: Solid State Phys.* **11** 783
[9] Chepin J and Ross J H 1991 *J. Phys.: Condens. Matter* **3** 8103
[10] Abragam A 1961 *The Principles of Nuclear Magnetism* (Oxford: Clarendon)
[11] Rega T 1991 *J. Phys.: Condens. Matter* **3** 1871
[12] Watanabe I 1994 *J. Phys. Soc. Japan* **63** 1560
[13] Suter A, Mali M, Roos J and Brinkmann D 1998 *J. Phys.: Condens. Matter* **10** 5977
[14] Rao B K, Subhadra K G and Sirdeshmuh D B 1981 *Indian J. Pure Appl. Phys.* **19** 87
[15] Cousi M, Vignalou J R and Boulton G 1976 *Solid State Commun.* **20** 461
[16] Nizhankovskii V I, Kharkovskii A I and Orlov V G 2002 *Ferroelectrics* at press
[17] Kharkovskii A I, Nizhankovskii V I, Kravchenko E A and Orlov V G 1996 *Z. Naturf.* a **51** 665